

P. H. Stone · M. S. Yao

## The ice-covered Earth instability in a model of intermediate complexity

Received: 4 March 2003 / Accepted: 6 February 2004 / Published online: 19 May 2004  
© Springer-Verlag 2004

**Abstract** The ice-covered Earth instability found in energy balance models is studied with a zonal mean statistical dynamical atmospheric model coupled to a global mixed layer ocean model. The response of the model to changes in solar constant is examined in two parallel studies, one with and one without a fixed meridional heat transport (a  $Q$ -flux) being included in the ocean model. The  $Q$ -flux is derived so as to make the climate with the current value of the solar constant resemble the earth's current climate. In both cases the climate displays a hysteresis loop as the solar constant decreases and then increases, with two equilibrium states being possible for a range of values of the solar constant. In the case without a  $Q$ -flux, as in energy balance models, one state corresponds to an ice-covered Earth, and the other is partially covered. In the case with a  $Q$ -flux, because the poleward  $Q$ -flux is stronger in the Southern Hemisphere, one state corresponds to an ice-covered Northern Hemisphere, but a Southern Hemisphere that is only partially ice-covered; the other state has much reduced ice-cover in both hemispheres. In the case when the  $Q$ -flux is present, the sensitivity of the state with smaller ice-cover is about half as much, and the hysteresis loop extends over a smaller range of values of the solar constant. Also in this case there is a strong ice-covered Earth instability that sets in when the solar constant is about 13–14% below the current value. However in the case without a  $Q$ -flux the ice-covered Earth instability virtually disappears. The different behavior is attributed to the much lower efficiency of the meridional heat transport in the case with no  $Q$ -flux.

The behavior in this case may be more realistic for cold climates. The results in both cases confirm the simple analytical relation between global mean surface temperature and global ice area found in energy balance models.

### 1 Introduction

The important role that ice-albedo-temperature feedback plays in determining climate sensitivity has been apparent since the pioneering work of Budyko (1969) and Sellers (1969). Using energy balance models (EBMs) they showed that this positive feedback enhances climate sensitivity and can cause multiple climate equilibria. Associated with these multiple equilibria in energy balance models are two different kinds of instability (North et al. 1981). In one, generally referred to as the small ice-cap instability (SICI), an ice cap which becomes sufficiently small loses stability and the climate passes to a state with no ice. In the other, generally referred to as the ice-covered Earth instability an ice cap which becomes sufficiently large also loses stability, and the climate passes to a state in which the whole globe is covered with ice. An obvious question of interest is whether these instabilities are robust, i.e., do they also occur in more sophisticated models?

In the case of the small ice-cap instability the answer appears to be no. In particular two studies with general circulation models (GCMs) have failed to find it (Crowley et al. 1994; Lee and North 1995). Crowley et al. (1994) did find a “behavior very similar to SICI,” in this case a greatly enhanced sensitivity due to the ice-(in their case snow-)albedo-temperature feedback, but they did not find an actual instability or the corresponding multiple equilibria.

There are many simplifications and approximations in EBMs which if relaxed can eliminate the SICI (North 1984). We note in particular that only EBMs that

---

P. H. Stone (✉)  
Department of Earth,  
Atmospheric and Planetary Sciences Massachusetts Institute  
of Technology, Cambridge, MA 02139, USA  
E-mail: phstone@mit.edu

M. S. Yao  
SGT, Goddard Institute for Space Studies National  
Aeronautics and Space Administration,  
New York, NY, USA

assume that the meridional heat transport in the climate system can be represented by linear diffusion contain the SICI. As first shown by Lin (1978) and explained by North (1984), if the heat transport is nonlinear, i.e., if it is more sensitive to the meridional temperature gradient than is implied by a linear diffusion law, then the SICI disappears. In fact meridional heat transports in mid and high latitudes are dominated by atmospheric eddy heat transports, and all theories of these transports lead to dependences that are nonlinear in this sense (Green 1970; Stone 1972; Held 1978; Branscome 1983; Held and Larichev 1996). Empirical studies also show that it is nonlinear (Stone and Miller 1980).

In any case, in the study presented here we use a two-dimensional (zonal mean) statistical dynamical atmospheric model (Stone and Yao 1990) in which the eddy heat transport is based on one of these nonlinear theories (Branscome 1983). Thus we would not expect the SICI to occur in our model, and as will be seen subsequently it does not.

By contrast the ice-covered Earth instability (ICEI) appears to be much less dependent on the simplifications and approximations used in EBMs. It also appears in radiative-convective equilibrium models (Wang and Stone 1980) and one study with an atmospheric GCM found multiple equilibria thus implying the possible presence of the ICEI. In particular Lee and North (1995), using an atmospheric GCM coupled to a "swamp" surface found two different states for the same solar forcing, one corresponding to an ice-covered Earth and the other with a small ice cap.

The existence of the ICEI would have important implications for paleoclimate studies, because it would imply the possibility that in earlier epochs, when the Sun was dimmer, the Earth should have been ice-covered. However the paleoclimate evidence indicates that during these epochs the Earth was generally not ice-covered (Crowley and North 1991). Whether this "faint young Sun paradox" is in fact a paradox and requires another forcing such as increased CO<sub>2</sub> concentrations to resolve it, depends on what the actual properties of the ICEI are. In addition there is evidence that there were at least a few periods in the Earth's early history when it may have been ice-covered, or nearly so (e.g., Hoffman et al. 1998). This has led some to propose the "snowball earth hypothesis," i.e., that these periods were caused by the ICEI (e.g., Kirschvink 1992). However it is not clear what forcing might have initiated these episodes. The relatively rapid changes associated with them cannot be explained by changes in the Sun's output-again, another forcing is required.

Evaluating what role the ICEI might play in paleoclimate changes requires a knowledge of how the Earth's possible equilibrium states depend on the forcing. A standard way of analyzing the possibilities is to calculate the hysteresis loop describing how the size of the polar ice cap varies with solar constant (North 1975). In particular, one would like to know what is the width of the hysteresis loop, and how is it

positioned with respect to current and past values of the solar constant? In this study we address these questions with a model that is considerably more sophisticated than the EBMs that have previously been used to address it.

---

## 2 Model description

The model used in this study is one of the class of models now generally referred to as Earth models of intermediate complexity (Claussen et al. 2002). The atmospheric model is a two-dimensional (2D) zonal mean model. It is based on the Model II general circulation model (GCM) of the Goddard Institute for Space Studies (GISS, Hansen et al. 1983). The model solves the primitive equations (including the moisture conservation equation) in sigma and spherical coordinates as an initial value problem. There are nine vertical layers: two in the planetary boundary layer, five in the troposphere, and two in the stratosphere. The model top is at 10 hPa, and at higher levels temperatures are determined by radiative equilibrium. There are 24 grid points in latitude, corresponding to a resolution of 7.826°. The time step is 20 min, and an eighth-order Shapiro filter is used to suppress the two-grid-size noise typical of 2D models. The filter is applied to potential temperature and surface pressure once every hour. Tests of the impact of the filter show that its contribution to the meridional heat transport is negligible, less than 0.1 PW.

Incident solar radiation is specified as a function of time of day, season, and latitude. The radiative calculations include all significant atmospheric constituents, and employ realistic shortwave and longwave properties. The distribution of water vapor is calculated, while the remaining radiatively active constituents are specified. Zonal mean cloud covers are taken from a simulation of the current climate with the GISS GCM, and are fixed in the experiments reported here.

Large-scale condensation and precipitation occur in an atmospheric layer whenever the relative humidity exceeds 100%. Moist convection occurs whenever the moist static energy at one level exceeds the saturated moist static energy at the next higher level. The convection is parametrized with a penetrative convection scheme which transports sensible heat, moisture, and horizontal momentum between the unstable layers. Any resulting supersaturation leads to condensation and precipitation. The amount of mixing due to moist convection depends on the fraction of a latitude belt which is unstable, and this is calculated from the zonal variance of the moist static energy. This variance is assumed to arise from eddies generated by baroclinic instability, and it is calculated from parametrizations based on baroclinic stability theory (see Yao and Stone 1987).

The large-scale eddy fluxes of momentum, heat, and moisture are also parametrized, based on the assumption that the eddies arise from baroclinic instability. The parametrizations and their performance are described in

Stone and Yao (1990 and Yao and Stone (1987)). There is no representation of stationary waves in the model.

In all the simulations reported here, the lower boundary is all ocean, with a sea-ice fraction at each latitude. The ocean is represented by a mixed layer model with its temperature calculated interactively. The depth of the mixed layer is specified and varies with latitude and season based on climatology (NOAA 1974; Gordon 1982). These depths are held fixed in all the simulations. The mixed layer temperature equation may or may not contain a source term calculated from the divergence of a specified and fixed meridional heat flux in the ocean. Surface fluxes of momentum, heat, and moisture are calculated separately at each latitude for each surface type using conventional drag laws. The fluxes for different surface types are then averaged together at each latitude before they interact with the atmosphere.

Sea ice is calculated from a simple thermodynamic ice model. When heat loss tends to drop the mixed layer temperature below  $-1.6^{\circ}\text{C}$ , the temperature is fixed at  $-1.6^{\circ}\text{C}$  and the heat loss in excess of that needed to maintain this temperature is used to form a layer of sea-ice 1 m deep. Further cooling increases the horizontal extent of the sea-ice until the grid point is filled. Further cooling increases the sea-ice depth. Leads are parameterized by requiring the fraction of open water in a gridbox to be  $\geq 0.06 \left(\frac{1}{z} - \frac{1}{5}\right)$ , where  $z$  is the depth of the sea-ice in meters. There are no leads when  $z > 5$  m. When the sea-ice starts to melt, the horizontal extent is reduced, while the depth is held constant. Temperature in the sea-ice is represented by a two-slab model, with parabolic profiles in each slab, and heat is exchanged with the mixed layer by conduction.

The albedoes of the ocean surface, sea-ice, and snow (which covers the sea-ice most of the time) are calculated from the algorithms given by Hansen et al. (1983). The albedo of the sea-ice/snow surfaces is generally in the range 0.45 to 0.55 at all latitudes, while the ocean surface albedo typically varies from 0.04 in low latitudes to 0.11 near the pole. The global mean planetary albedo calculated by the model varies from 0.29 when the planet is ice free to 0.51 when it is ice covered.

### 3 Control runs

We constructed two control runs, one in which there is no heat transport in the ocean model, and one in which a heat transport is specified. This specified heat transport, sometimes called a “ $Q$ -flux,” was calculated from a simulation with the atmospheric model forced by seasonally varying sea-surface temperatures and sea-ice fractions taken from zonal means of the current ocean climatology. Heat storage is taken into account and the  $Q$ -flux’s divergence is smoothed with a second-order Shapiro filter. Thus, by construction, the  $Q$ -flux is the ocean heat transport necessary for the model to reproduce the current sea-surface climatology when the

mixed-layer temperatures and sea-ice are calculated interactively.

Not surprisingly, given our model’s simplifications, the global mean annual mean net surface heat flux in the simulation used to calculate the  $Q$ -flux is not zero. Thus an additional initial adjustment has to be made before the  $Q$ -flux is calculated. In particular, we make a uniform adjustment of  $-7.38\%$  in the solar radiation incident at the surface so as to remove the net global mean annual mean surface heat flux. Then the remaining residual net surface heat flux at each latitude and season is used to calculate the  $Q$ -flux, while taking into account the heat storage in the mixed layer and the sea-ice. The annual mean of the convergence of the  $Q$ -flux is shown in Fig. 1. Qualitatively it corresponds to a flux of heat from low to high latitudes in the ocean in both hemispheres. Quantitatively the implied poleward heat fluxes differ from those in the current climate because of the model’s simplifications, e.g., its surface being all ocean. Nevertheless in this simulation the global mean planetary albedo is 0.30, the same as the Earth’s observed albedo.

In the control run with no  $Q$ -flux, the uniform adjustment of the incident solar radiation is retained. Thus the differences between the two sets of climate change experiments reported in the next section will be due entirely to the presence or absence of the  $Q$ -flux. Figure 2 compares the sea-surface temperatures in the two control runs. (Note that in all our figures and discussion of “sea-surface temperatures,” in regions where sea-ice has formed this refers to the surface temperature of the sea ice.) Because of the absence of the poleward heat transport of the ocean in the case with no  $Q$ -flux, much more sea-ice forms in the polar regions. The area of sea-ice increases when the  $Q$ -flux is removed from 8% to 48% in the Northern Hemisphere, and from 12% to 48% in the Southern Hemisphere. The asymmetry between the two hemispheres when the  $Q$ -flux is present is primarily due to the asymmetry in the  $Q$ -flux (see Fig. 1) and it virtually disappears when the  $Q$ -flux is removed. (There remain small asymmetries associated with

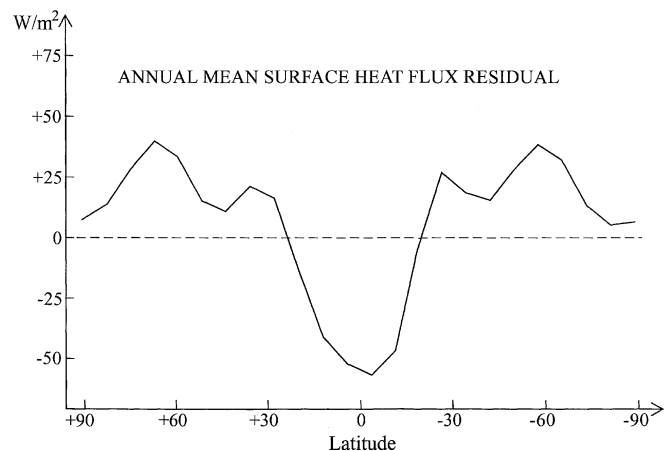
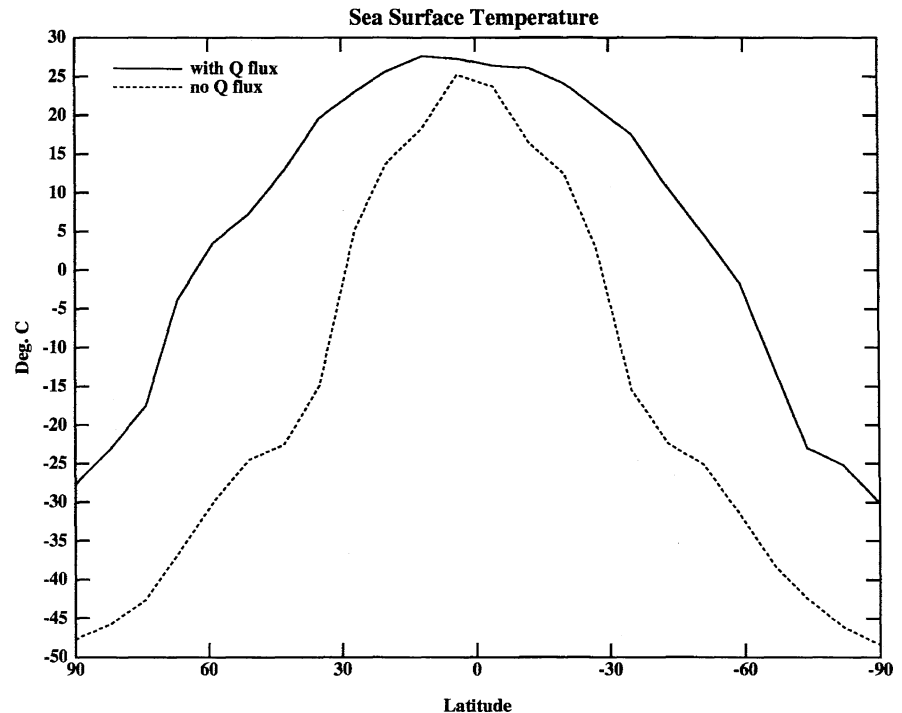


Fig. 1 Convergence of the  $Q$ -flux per unit surface area versus latitude

**Fig. 2** Sea surface temperature versus latitude in the two control runs: with  $Q$ -flux (solid curve) and without  $Q$ -flux (dashed curve)



asymmetries in the specified cloud and mixed-layer depth distributions.) The larger global mean planetary albedo associated with the greater amount of sea-ice in the case with no  $Q$ -flux causes considerable global cooling, so that even tropical temperatures are slightly lower.

#### 4 Effect of changes in the solar constant

##### 4.1 With $Q$ -flux

Figure 3 shows the equilibrium position of the equatorward boundary of the sea-ice in both hemispheres, expressed as the sine of the latitude of the boundary,  $X_S$ , versus solar constant,  $S$ . (Thus the fractional area occupied by sea-ice in each hemisphere,  $A$ , is given by  $1 - X_S$ .) For large values of the solar constant there is no sea-ice in either hemisphere. As  $S$  decreases, sea-ice first appears in the Southern Hemisphere, because the  $Q$ -flux supplies more heat to polar regions in the Northern Hemisphere than in the Southern Hemisphere (see Fig. 1). As  $S$  decreases further, the amount of sea-ice increases more rapidly in the Northern Hemisphere, because the  $Q$ -flux supplies more heat to mid-latitudes in the Southern Hemisphere (see Fig. 1). An ice-covered Earth instability (ICEI) sets in when  $S$  decreases to a value about 13–14% below the current value, and for smaller values the planet is covered with ice.

If the solar constant increases from small values, the Northern Hemisphere remains essentially ice covered until  $S$  reaches a value about 2% below the current value. However the sea-ice in the Southern Hemisphere starts to increase at lower values of  $S$ , at values between

10 and 14% below the current value. Thus there are two distinct equilibrium states for values of the solar constant ranging between  $13\frac{1}{2}\%$  and 2% below the current value. However the hemispheric ice covers differ because of the asymmetry in the  $Q$ -flux. Nevertheless the two states are clearly analogous to those in EBMs, with one having relatively little ice-cover, like the current climate, and the other being mostly ice covered, essentially 100% in the Northern Hemisphere, and more than 50% in the Southern Hemisphere.

The main value of including a  $Q$ -flux is that it yields surface temperatures near those of the current climate (see Fig. 2), so that the important feedbacks in the system that depend on temperature will have strengths that are realistic for the current climate. In particular the strength of the water-vapor- and ice-albedo-temperature feedbacks will be similar to their strengths as parametrized in simpler models. Figure 4 shows how the hemispheric mean sea surface temperatures vary with solar constant in the same equilibrium states as those shown in Fig. 3. The conventional measure of sensitivity of climate to changes in solar constant is the beta-parameter

$$\beta = S \frac{dT_{G1}}{dS},$$

where  $T_{G1}$  is the global mean sea-surface temperature. In EBMs, if one assumes that the structure of the climate system is fixed, for  $S = S_0$ ,  $\beta \approx 70^\circ$ , while if one includes water-vapor- and ice-albedo-temperature feedbacks using conventional parametrizations,  $\beta$  is increased to  $\beta \approx 120^\circ$  to  $140^\circ$  (Wang and Stone 1980).

If we use the results shown in Fig. 4, for  $S = S_0$  we calculate  $\beta \approx 165^\circ$  for the Northern Hemisphere,  $\beta \approx$

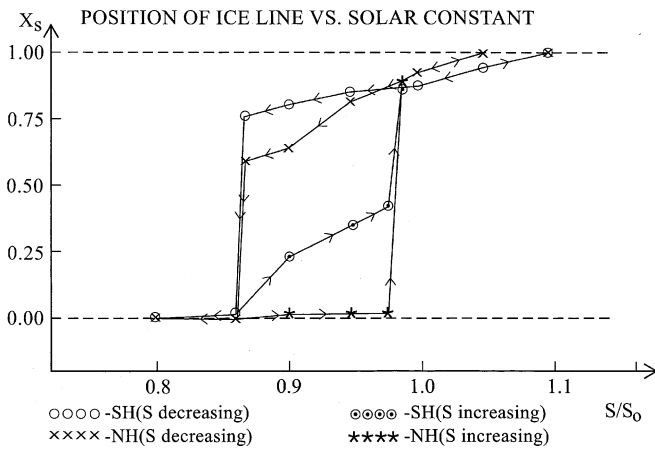


**Fig. 3** Sine of the latitude ( $X_s$ ) at the boundary of the sea-ice in both hemispheres versus the solar constant normalized by its current value  $S_0 = 1367 \text{ W/m}^2$ . The  $X_s$ 's and circles indicate the boundary in the Northern and Southern Hemispheres, respectively, when the solar constant decreases from large values. The stars and the circles containing dots indicate the boundaries in the Northern and Southern Hemispheres, respectively, when the solar constant increases from small values. The calculated points have been joined, somewhat arbitrarily, by straight lines with arrows to make the hysteresis loops in the two hemispheres clearer

120° for the Southern Hemisphere, and  $\beta \approx 145^\circ$  for the global mean. The sensitivity of the Southern Hemisphere is smaller in spite of its larger ice area when  $S = S_0$ , because of the Southern Hemisphere's stronger mid-latitude warming due to the asymmetric  $Q$ -flux. Clearly a  $Q$ -flux affects the climate sensitivity, as would any flux adjustment (Marotzke and Stone 1995), because it constrains temperature changes. Nevertheless the model's sensitivity is similar to that of EBMs. It is also similar to that of coupled GCMs. In particular, we note that the model's sensitivity with the  $Q$ -flux to a doubling of  $\text{CO}_2$  is 2.2 °C, similar to that of many coupled GCMs (Albritton et al. 2001).

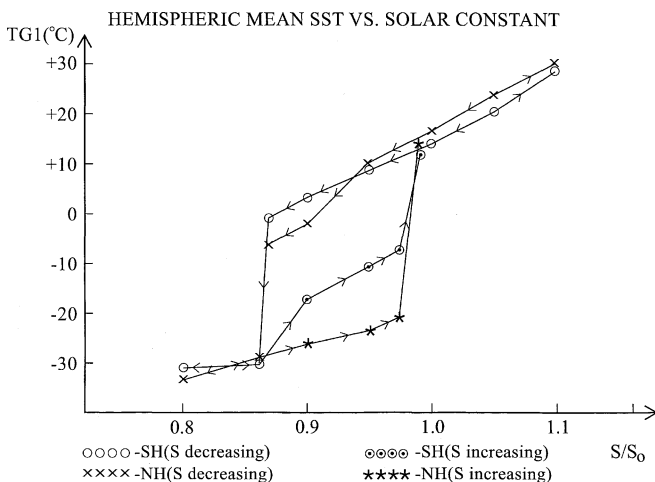


**Fig. 4** Same as Fig. 3, but hemispheric mean sea surface temperature versus normalized solar constant

### 4.2 Without $Q$ -flux

Figure 5 shows how the equilibrium values of  $X_s$  vary with  $S$  when no  $Q$ -flux is included in the model. The two hemispheres now behave in a closely symmetric fashion, so only a single value of  $X_s$  is shown for each equilibrium state. If we again start from the ice-free states for large  $S$ , as  $S$  decreases ice first appears for values of  $S$  about 12% greater than the current value. This is noticeably larger than the value at which it starts to form when the  $Q$ -flux is present. In the latter case ice only started to form at a value 8% larger than the current value, because of the high-latitude warming associated with the  $Q$ -flux. Similarly, for  $S = S_0$ , there is much more sea-ice present without the  $Q$ -flux, 48% vs. a global mean of 10% with the  $Q$ -flux.

As  $S$  decreases further, the area of ice increases monotonically until  $S$  reaches a value about 14% below the current value, when the planet becomes ice-covered. Whether there is a small ICEI at approximately this point, i.e., one in which  $X_s$  unstably decreases from a small value of  $X_s$  to  $X_s = 0$ , is not resolved by our experiments. In any case, it is apparent that in this case the ICEI has essentially disappeared. There is however still a second branch of equilibrium solutions which are completely ice covered and extend to larger values of  $S$ . This branch, which was found by increasing  $S$ , once an ice-covered equilibrium state had been found, is also illustrated in Fig. 5. This branch extends up to a value of  $S$  about 6% greater than the current value. Thus in the case without a  $Q$ -flux, the ICEI disappears or almost disappears, and the hysteresis loop is wider and now includes the current value of the solar constant.

Figure 6 shows the global mean sea-surface temperature vs. solar constant for the equilibrium states with no  $Q$ -flux. This figure illustrates that the climate sensitivity is greater for the states with non-global ice covers than for the ice-covered states. This was also true in the

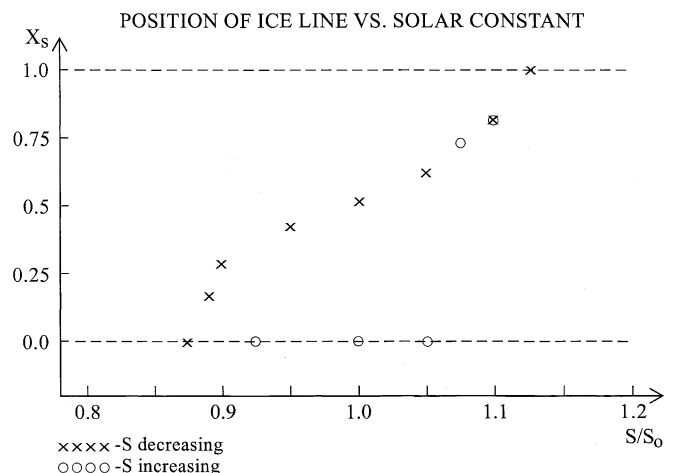


**Fig. 5**  $X_s$  versus normalized solar constant from the experiment with no  $Q$ -flux. The  $X_s$ 's indicate states found when  $S$  decreases from large values, and the circles indicate states found when  $S$  increases from small values

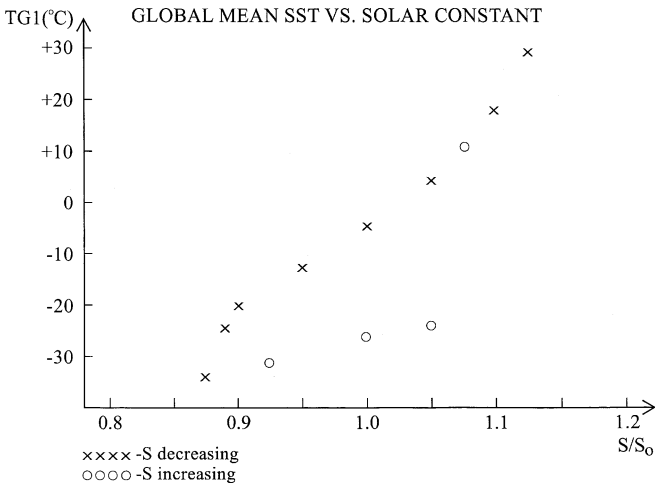


Fig. 6 Same as Fig. 5, but global mean sea surface temperature versus normalized solar constant

case with  $Q$ -flux (see Fig. 4), although the difference was less pronounced. From the results shown in Fig. 6 we calculate that the sensitivity,  $\beta$ , for the current value of the solar constant, is  $170^\circ$  for the state with partial ice cover and only  $60^\circ$  for the ice-covered state. Thus the sensitivity for the partially ice-covered states is greater without a  $Q$ -flux than with it. This is even more true if we compare the sensitivity of the partially ice-covered states in the two cases for states which have the same global mean sea-surface temperature. For example, for states with global mean sea surface temperatures of  $15^\circ\text{C}$ ,  $\beta \approx 145^\circ$  in the case with the  $Q$ -flux and  $270^\circ$  without the  $Q$ -flux.

The qualitative difference between the cases with and without a  $Q$ -flux can be explained by the differences in the efficiency of the meridional heat transport in the two cases. The efficiency, as measured by an effective diffusion coefficient for the heat transport, is considerably less in the case without a  $Q$ -flux, first because there is no oceanic contribution to the heat transport, and second because, for a given value of the solar constant, the climate is a lot colder (see Fig. 2), and thus there is much less contribution to the heat flux in the form of latent heat. Held and Suarez (1974) examined how the solution of an EBM depends on the transport efficiency, and showed that when it decreases the behavior changes from one like that shown in Fig. 3 to one like that shown in Fig. 5. In particular, as the efficiency decreases, the climate sensitivity of the current climate increases, and the ICEI decreases, and even disappears in the limit of zero efficiency.

### 5 The relationship between global mean temperature and ice-cover

Wang and Stone (1980) pointed out that the global mean ice cover in EBMs is much more sensitive to global mean surface temperature than to the temperature contrast

between low and high latitudes. This allowed them to derive a simple expression relating  $T_{G1}$  in degrees C and  $X_s$ , namely

$$T_{G1} = T_c - \frac{1}{2}T_2(3X_s^2 - 1), \quad 0 \leq X_s \leq 1, \quad (1)$$

where  $T_c$  and  $T_2$  are constants, tuned to the model's current climate. In particular  $T_c$  is the annual mean temperature (degrees C) at the annual mean position of the ice-line, and  $T_2$  is the coefficient (in degrees C) of the second order Legendre polynomial in an expansion of the annual mean zonal mean surface temperature. (Thus the equator-to-pole temperature contrast is approximately  $\frac{3}{2}T_2$ .) This expression allows one to include the ice-albedo-temperature feedback in radiative-convective equilibrium models, and their results then agree quite well with the Budyko-Sellers kind of EBM (Wang and Stone 1980).

We use the results from our two sets of experiments to test whether Eq. (1) still holds for the more sophisticated model used here. For each of the two sets of experiments  $T_c$  and  $T_2$  were calculated from the equilibrium states when  $S = S_0$ . For the experiments with the  $Q$ -flux we calculate  $T_c = -6.04^\circ\text{C}$ ,  $T_2 = -29.5^\circ\text{C}$ , and therefore Eq. (1) becomes

$$X_s^2 = 0.0226T_{G1} + 0.470, \quad 0 \leq X_s \leq 1. \quad (2)$$

Figure 7 shows the fraction of the globe covered by ice,  $A$ , versus  $T_{G1}$  from this equation and from the model calculations with the  $Q$ -flux. For the case without  $Q$ -flux, the corresponding values of the constants are  $T_c = -0.05^\circ\text{C}$  and  $T_2 = -48.5^\circ\text{C}$ , and the parametrization becomes

$$X_s^2 = 0.0138T_{G1} + 0.333, \quad 0 \leq X_s \leq 1. \quad (3)$$

Figure 8 shows the comparison for the case without a  $Q$ -flux. We note that the parametrization has been tuned to quite a different climate in this case. Nevertheless we see

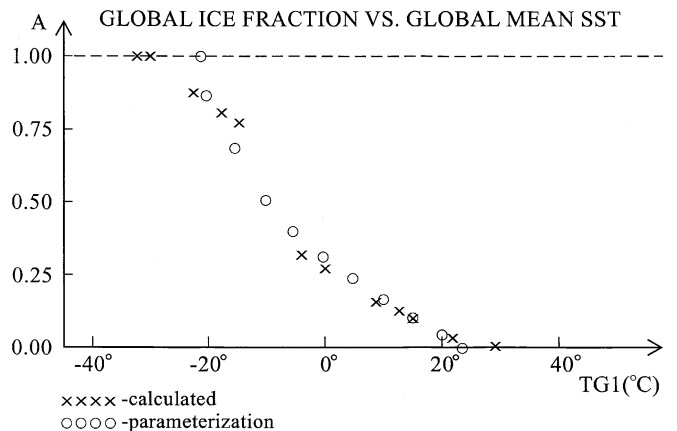
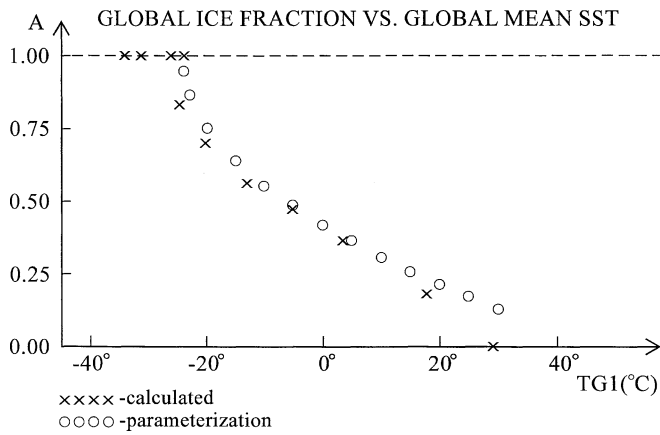


Fig. 7 Fraction of the global area covered by sea-ice versus global mean sea-surface temperature. Results from the model with  $Q$ -flux are shown by the X's, and results from the parametrization, Eq. (2), by the circles



**Fig. 8** Same as Fig. 7, except the model results are without a  $Q$ -flux and the parametrization is given by Eq. (3)

that the model calculations and the parametrization agree quite well throughout most of the range of  $A$  in both cases. The one exception is the case without a  $Q$ -flux when  $A \leq 0.2$ .

## 6 Summary and discussion

We have used an earth model of intermediate complexity to see if the ice-covered Earth instability found in EBMs also occurs in the more sophisticated model. It does, when a  $Q$ -flux tuned to the current climate is included. All the additional physics that is included in our model does not change the basic qualitative behavior that results from the introduction of the ice-albedo-temperature feedback in EBMs. The details of the hysteresis loop and the ICEI do depend on details of the model's formulation, as illustrated by the differences in our results with and without a  $Q$ -flux, but the additional physics included in our model does not resolve the "faint young Sun paradox."

Our results can also be compared with those of Lee and North (1995). They used the NCAR CCMO GCM coupled to a global land surface with no topography and fixed soil moisture. Thus there was no ocean heat transport in their model, and we may compare their results with ours without the  $Q$ -flux. They reported that for  $S = S_0$  they only found an ice-covered Earth solution, while for  $S = 1.2S_0$  they found both an ice-free and an ice-covered earth solution. This implies that their model did have a hysteresis loop for  $S > S_0$ . By contrast our hysteresis loop in the absence of the  $Q$ -flux occurred over the range  $0.88 S_0 \lesssim S \lesssim 1.06S_0$ .

One difference between Lee and North's (1995) simulation and ours was that they forced their model with the annual mean insolation and omitted any seasonal cycle. However this does not appear to be the cause of the difference in our results because in our simulations with values of the solar constant in the range explored by Lee and North ( $S \sim 1.10 S_0$ ) there is no significant seasonal cycle in the area of the sea-ice. One possible

source of the differences in our results is our use of ocean surfaces rather than land surfaces when ice is not present. The former has a lower albedo and will thus cause a warmer climate for a given value of the solar constant. Increasing the ice-free albedo would shift the hysteresis loop in Fig. 5 to the right towards the hysteresis loop implied by Lee and North's (1995) results.

There are two particular sets of feedback processes left out of our model that could potentially have a major impact on the ICEI and the hysteresis loop. One is cloud feedback, which unfortunately is poorly understood at this time (Albritton et al. 2001). The other is ocean dynamics, which is responsible for substantial heat transport and thus interacts with the ice-albedo-temperature feedback (Poulson et al. 2001). This interaction is likely to change when the solar constant changes. To include this effect would require an ocean GCM. Because of the very long equilibration times of the ocean, including an OGCM in a study like ours would require a large computational expense.

For small changes in the solar constant we would expect our results with the  $Q$ -flux to be fairly accurate because the sensitivity of the model for  $S \approx S_0$  is similar to that of coupled GCMs. However, for the situation where the planet is ice covered, or nearly so, the simulated fluxes of heat and moisture into the ocean will be greatly reduced. Since the oceanic heat transport is associated primarily with the thermohaline circulation driven by these fluxes, we would expect the ocean heat transport to be reduced when the Earth is ice covered, or nearly so. Thus we suggest that interactive ocean dynamics would move the left-most segment of the upper branch of the hysteresis loop in Fig. 3 downward, and decrease the amplitude of the ice-covered Earth instability, making the hysteresis loop more like that without any  $Q$ -flux shown in Fig. 5. Indeed our results raise the possibility that in colder climates the ICEI may not exist if the ocean heat transport becomes sufficiently weak. This possibility needs to be investigated with a climate model which includes an ocean GCM.

**Acknowledgements** We are indebted to Dr. M.A.M. Maqueda for a helpful review of an earlier version of this paper.

## References

- Albritton DL, Meira Filho LG, Cubasch U, Dai X, Ding Y, Griggs DJ, Hewitson B, Houghton JT, Isaksen I, Karl T, McFarland M, Meleshko VP, Mitchell JFB, Noguer M, Nyenzi BS, Oppenheimer M, Penner JE, Pollonais S, Stocker T, Trenberth KE (2001) Technical summary. In: Houghton JT et al. (eds). Climate change 2001: the scientific basis. Cambridge University Press, UK, pp 881
- Branscome LE (1983) A parametrization of transient eddy heat flux on a beta-plane. *J Atmos Sci* 40: 2508–2521
- Budyko MI (1969) The effect of solar radiation variations on the climate of the earth. *Tellus* 21: 611–619
- Claussen M, Mysak L, Weaver A, Crucifix M, Fichefet T, Loutre M, Weber S, Alcamo J, Alexeev V, Berger A, Calov R, Ganapolski A, Goosse H, Lohman G, Lunkeit F, Mokhov I,

- Petoukhov V, Stone P, Wang Z (2002) Earth system models of intermediate complexity: closing the gap in the spectrum of climate system models. *Clim Dyn* 18: 579–586
- Crowley TJ, North GR (1991) *Paleoclimatology*. Oxford University Press, New York, pp 339
- Crowley TJ, Yip KJ, Baum SK (1994) Snowline instability in a general circulation model: application to Carboniferous glaciation. *Clim Dyn* 10: 363–376
- Gordon AL (1982) *Southern Ocean Atlas*. Columbia University Press, New York, pp 34
- Green JSA (1970) Transfer properties of the large-scale eddies and the general circulation of the atmosphere. *Q J R Meteorol Soc* 96: 157–185
- Hansen J, Russell G, Rind D, Stone P, Lacis A, Lebedeff S, Ruedy R, Travis L (1983) Efficient three-dimensional global models for climate studies: models I and II. *Mon Weather Rev* 111: 609–662
- Held IM (1978) The vertical scale of an unstable baroclinic wave and its importance for eddy heat flux parametrization. *J Atmos Sci* 35: 572–576
- Held IM, Larichev V (1996) A scaling theory for horizontally homogeneous, baroclinically unstable flow on a beta plane. *J Atmos Sci* 53: 946–952
- Held IM, Suarez MJ (1974) Simple albedo feedback models of the icecaps. *Tellus* 26: 613–627
- Hoffman PF, Kaufman AJ, Halverson GP, Schrag DP (1998) A neoproterozoic snowball earth. *Science* 281: 1342–1346
- Kirschvink JL (1992) Late proterozoic low-latitude global glaciation: the Snowball Earth. In: Schopf JW, Klein C (eds) *The Proterozoic biosphere*, Cambridge University Press, Cambridge UK, pp 51–52
- Lee W-H, North GR (1995) Small ice cap instability in the presence of fluctuations. *Climate Dyn* 11: 242–246
- Lin CA (1978) The effect of nonlinear diffusive heat transport in a simple climate model. *J Atmos Sci* 35: 337–340
- Marotzke J, Stone PH (1995) Atmospheric transports, the thermohaline circulation, and flux adjustments in a simple coupled model. *J Phys Ocean* 25: 1350–1364
- NOAA (1974) *User's Guide to NODC Data Services*, Environmental Data Service. Washington, DC, USA
- North GR (1984) The small ice cap instability in diffusive energy balance climate models. *J Atmos Sci* 41: 3390–3395
- North GR, Cahalan RF, Coakley JA Jr (1981), Energy balance climate models. *Rev Geophys Space Phys* 19: 91–121
- North (1975) Analytical solution to a simple climate model with a diffusive heat transport. *J Atmos Sci* 32: 1301–1307
- Poulsen CJ, Pierrehumbert RT, Jacob RL (2001) Impact of ocean dynamics on the simulation of the Neoproterozoic “snowball earth.” *Geophys Res Lett* 28: 1575–1578
- Sellers WD (1969) A global climatic model based on the energy balance of the earth-atmosphere system. *J Appl Meteor* 8: 392–400
- Stone PH (1972) A simplified radiative-dynamical model for the static stability of rotating atmospheres. *J Atmos Sci* 29: 405–418
- Stone PH, Miller D (1980) Empirical relations between seasonal changes in meridional temperature gradients and meridional fluxes of heat. *J Atmos Sci* 37: 1708–1721
- Stone PH, Yao M-S (1990) Development of a two-dimensional zonally averaged statistical-dynamical model. Part III: the parametrization of the eddy fluxes of heat and moisture. *J Clim* 3: 726–740
- Wang W-C, Stone PH (1980) Effect of ice-albedo feedback on global sensitivity in a one-dimensional radiative-convective climate model. *J Atmos Sci* 37: 545–552
- Yao M-S, Stone PH (1987) Development of a two-dimensional zonally averaged statistical-dynamical model. Part I: the parametrization of moist convection and its role in the general circulation. *J Atmos Sci* 44: 65–82